Environ Monit Assess (2021) 193: 45
https://doi.org/10.1007/s10661-020-08788-z

Evaluation of the MOD11A2 product for canopy temperature monitoring in the Brazilian Atlantic Forest

Melina Daniel de Andrade · Rafael Coll Delgado · Sady Júnior Martins da Costa de Menezes · Rafael de Ávila Rodrigues · Paulo Eduardo Teodoro · Carlos Antonio da Silva Junior · Marcos Gervasio Pereira

Received: 6 May 2020 / Accepted: 30 November 2020 / Published online: 7 January 2021

Abstract Forest canopies have an important influence on the global climate balance. Through the analysis of the temperature of the canopy, it is possible to infer about the physiological aspects of the plants, helping to understand the behavior of the vegetation and, consequently, in the environmental monitoring and management of green areas. This study aims to validate the MOD11A2 V006 product from canopy surface temperature data obtained by an infrared radiation sensor. For the validation of the MOD11A2 product, a comparative analysis was performed between the land surface temperature (LST) data, obtained by the MODIS sensor, and the canopy temperature data, obtained by the SI-111 infrared radiation sensor coupled to the Itatiaia National Park (PNI) micrometeorological tower. Meteorological variables and land surface temperature collected from January to December 2018 in the PNI were also analyzed. The results reveal that the MOD11A2 product overestimates the canopy temperature in the daytime (MB ranging from 1.56 to 3.57 °C) and underestimates in the night time (MB ranging from − 0.18 to − 4.22 °C). During daytime, the months corresponding to the dry season presented a very high correlation (r = 0.74 and 0.86) and the highest values for the Willmott index (d = 0.70 and 0.64). At nighttime, the MOD11A2 product did not present a good performance for the LST estimation, especially in the rainy season. Therefore, we observed that the MOD11A2 product has limitations to estimate the land surface temperature and that possible changes in the algorithm of this product can be performed for high atmospheric humidity conditions.

Keywords Environmental satellite · Biophysical parameters · Conservation unit · Digital sensors

M. D. de Andrade · R. C. Delgado
Department of Environmental Sciences, Forest Institute, Federal Rural University of Rio de Janeiro (UFRRJ), Seropédica, Rio de Janeiro 23897-000, Brazil

S. J. M. da Costa de Menezes
Department of Environmental Sciences, Três Rios Institute, Federal Rural University of Rio de Janeiro (UFRRJ), Três Rios, Rio de Janeiro 25802-100, Brazil

R. de Ávila Rodrigues
Special Academic Unit Institute of Geography, Federal University Catalão, Goiás 75704-020, Brazil

P. E. Teodoro
Department of Crop Science, Federal University of Mato Grosso do Sul (UFMS), Chapadão do Sul, Mato Grosso do Sul 79560-000, Brazil

C. A. da Silva Junior (✉)
Department of Geography, State University of Mato Grosso (UNEMAT), Sinop, Mato Grosso 78555000, Brazil
e-mail: carlosjr@unemat.br

M. G. Pereira
Department of Soils, Federal Rural University of Rio de Janeiro (UFRRJ), Seropédica, Rio de Janeiro 23897-000, Brazil

Introduction

Forest canopies are responsible for a significant portion of the gas and water vapor exchanges that occur in the atmosphere and on the land surface (Dixon et al. 1994),

having an important influence on the balance of the global climate. The canopy temperature is characterized as the result of the energy balance of the canopy, driven by climate conditions, canopy architecture, and plant transpiration (Song et al. 2017). It is closely linked to physiological processes such as respiration, evapotranspiration (Çamoğlu 2013; Colaizzi et al. 2017), CO2 assimilation (Gray et al. 2016; Kim et al. 2016), and photosynthesis (Helliker et al. 2018).

Canopy temperature measurements represent a useful approach for the interpretation and integration of biochemical, physiological, hydrological, and biogeochemical processes in forests (Kim et al. 2016). Orbital land surface temperature (LST) data are used to measure canopy temperature in agriculture (Heft-Neal et al. 2017) and forest (Gomis-Cebolla et al. 2018) ecosystems. Thermal infrared remote sensing provides a single method for acquiring surface temperature information at regional and global scales (Li et al. 2014) and is an important tool for the spatial and temporal understanding of this variable.

One of the main instruments used for obtaining surface temperature is the MODIS sensor (Moderate Resolution Imaging Spectroradiometer), developed by NASA (National Aeronautics and Space Administration). MODIS sensor LST products (MOD11) (Wan 2006) cover the day and night times and are used in several scientific fields.

However, orbital surface temperature data is not widely used by weather operational centers (Li et al. 2014). This can be explained by the fact that thermal infrared remote sensing measurements require atmospheric and surface emissivity corrections, which are usually associated with high uncertainties (Hulley et al. 2012), besides factors such as the spatial heterogeneity of the land surface, which makes data recovery and interpretation difficult (Guillevic et al. 2012). Thus, the validation of these products is an essential step in establishing their applicability and accuracy and can be performed through comparison with in situ measurements obtained, for example, by infrared radiation sensors.

Sensors sensitive to infrared wavelength radiation are ideal for measuring surface temperature in applications requiring extreme accuracy and no target interference due to their long wavelength (APOGEE 2018), used in several works to validate temperature data from the land surface obtained by remote sensing. Li et al. (2014) validated LST data obtained by the MODIS sensor through comparisons with measurements performed in the field by infrared radiometer for an arid area in Northwest China. The results showed that the MODIS sensor data underestimate LST in the studied area. The same result was obtained by Pérez-díaz et al. (2017) for the snow-covered surface in Caribou, USA. For forest-covered areas in the Peruvian Amazon, it was observed that LST data were overestimated by the MODIS sensor (Gomis-Cebolla et al. 2018).

The biome studied is an area of high biodiversity and one of the most threatened on the planet; in the Atlantic Forest area, no studies have yet been carried out to validate orbital LST data; i.e., there is still no specific information on the applicability of the MODIS product of land surface temperature for this region. As this is a highly threatened area of relevant interest for scientific research, and for knowing the difficulties encountered in field expeditions for data collection, the validation of orbital LST data is necessary, thus ensuring its use and hence helping in the understanding of the ecological processes that occur in these locations quickly, without requiring excessive expenditure and without negatively impacting the local fauna and flora.

However, many questions still need to be answered: (i) Were the infrared radiation sensors installed in the Itatiaia National Park able to validate the MOD11A2 V006 product data? (ii) What is the difference between the validations during night and day? (iii) Were the data influenced by time series, seasonality, and land cover? To answer these questions, this study validated the land surface temperature data of the product MOD11A2 V006 from canopy surface temperature data obtained from an infrared radiation sensor installed in an area of the Atlantic Forest in the Itatiaia National Park, Brazil.

Material and methods

Characterization of the study area

The study was carried out at Itatiaia National Park (PNI), the first full protection conservation unit (CU) in Brazil, constituted on June 14, 1937. The PNI is located in Serra da Mantiqueira, covering the municipalities of Bocaina de Minas and Itamonte, in the state of Minas Gerais (MG), and the

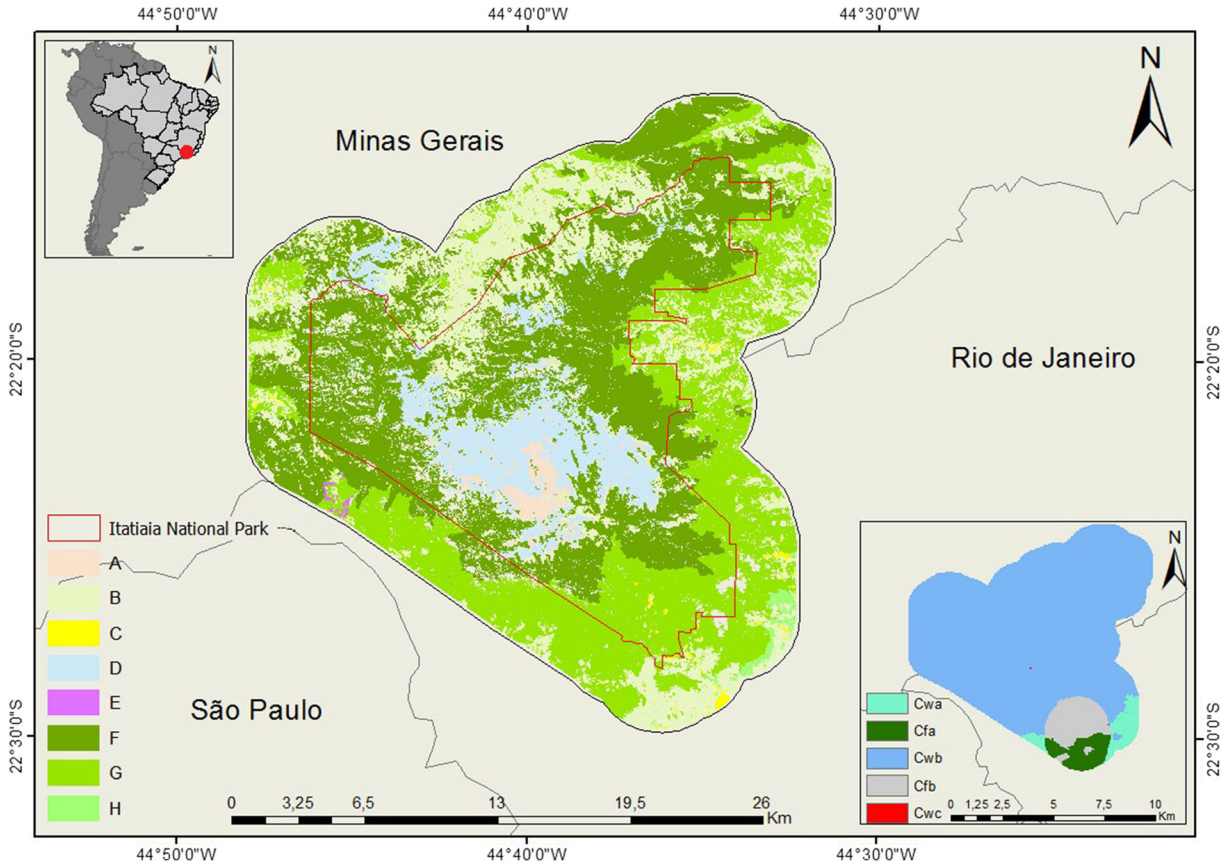

Fig. 1 Geographic location of the study area, Köppen climate domain, and land use and occupation. (**A**) Rocky outcrop, (**B**) agriculture, (**C**) urban area, (**D**) altitude fields, (**E**) planting areas, (**F**) dense ombrophilous high montane forest, (**G**) dense ombrophilous montane forest, and (**H**) dense ombrophilous sub-montane forest

municipalities of Itatiaia and Resende, in the state of Rio de Janeiro (RJ) (Barreto et al. 2013) (Fig. 1). It comprises an area of 28,086.00 ha, with mountainous relief with large rocky outcrops and altitudes varying from approximately 540.00 to 2791.55 m at its highest point, Pico das Agulhas Negras, the fifth highest in the country (Barreto et al. 2013).

According to the new Köppen classification for Brazil (Alvares et al. 2013), the park has five climatic domains, which are humid tropical without dry season with hot summer (Cfa); humid tropical without dry season with temperate summer (Cfb); humid tropical with dry winter and hot summer (Cwa); humid tropical with dry winter and temperate summer (Cwb); and humid tropical with dry winter and short and cool summer (Cwc).

The average annual rainfall is 215.00 mm and 149.00 mm, in the stations Agulhas Negras and Parque Itatiaia, respectively. Rains are scarcer from the end of April to October, with the minimum rainfall occurring in June and August with averages below 50.0 mm. In the months of June and July, the relative humidity does not exceed the average of 70.0%. The maximum absolute humidity occurs in December with 83.0%, and the minimum in June with 62.0% and the average is 75.2% (Barreto et al. 2013).

The PNI is entirely inserted in the Atlantic Forest biome covering plant formations of the dense ombrophilous forest, delimited by the sub-montane (from 100.00 to 600.00 m), montane (from 600.00 to 2000.00 m), and high montane (above 2000.00 m) (IBGE 2012) altimetry ranges. According to Delgado et al. (2018) considering a 3-km buffer, besides the forest areas, in the park, there are 5 other land use and occupation differentiations, classified from IKONOS high-resolution images (1 m—panchromatic and 4 m—multispectral) from July 2011 (Hiparc 2011) (Fig. 1 and Table 1).

Table 1 Land use and land cover classes, abbreviation, and coverage area

Land use and land cover	Abbreviation	Area (km^2)	%
Rocky outcrop	A	11.23	2.0
Agriculture	B	125.15	22.4
Urban area	C	2.97	0.5
Altitude fields	D	51.49	9.2
Planting areas	E	0.56	0.1
Dense ombrophilous high montane forest	F	208.64	37.4
Dense ombrophilous montane forest	G	154.86	27.8
Dense ombrophilous sub-montane forest	H	3.11	0.6
Total		558.01	100

Database

MODIS product

Daytime and nighttime land surface temperature data from the product MOD11A2 V006 (Wan 2013) produced and made available by NASA were used (https://search.earthdata.nasa.gov/). The MOD11A2 product is formed from the average of all LST observations in a clear sky condition of the MOD11A1 product over 8 days, and it was chosen by providing images with fewer invalid pixels due to cloud contamination. It has a spatial resolution of 1 × 1 km, in a tile of 1200 × 1200 km. The period analyzed was from January 1 to December 31, 2018, and 92 images from MOD11A2 product were used, tile h13v11.

The files are available in Raster in HDF format and sinusoidal projection. To acquire the images from the NASA servers and convert the cartographic projection to UTM WGS 84 and file format to .GeoTIFF, the MODIStsp package was used (Busetto and Ranghetti 2016) in the R software. Additionally, using the ArcGis 10.5 software, the files were converted to biophysical values (through multiplication by the scale factor 0.02) in degrees Celsius.

Some images had no value pixels because of cloud contamination. To fill these gaps, the interpolation by ordinary Krigagem was used. For this procedure, all the original images were cut, resulting in images of 245 × 137 pixels, with the Itatiaia National Park area in the center. For these images, the exponential (Eq. 2), spherical (Eq. 3), and Gaussian (Eq. 4) theoretical models were adjusted and tested, and the spatial dependency degree (SDD) (Eq. 5) was verified using the methodology proposed by Cambardella et al. (1994), where SDD with values ≤ 25% data have strong spatial dependence; SDD between 25 and 75% show moderate spatial dependence; SDD ≥ 75% have weak spatial dependence; and in SDD equal to 100%, the variable is spatially independent.

$$\widehat{\gamma}(h) = C_0 + C\left[1 - e^{\left(-\frac{h}{a}\right)}\right] \tag{1}$$

$$\widehat{\gamma}(h) = C_0 + C\left[1.5\frac{h}{a} - 0.5^{\left(\frac{h}{a}\right)^3}\right] \text{ if } : h < a$$
$$\widehat{\gamma}(h) = C_0 + C \text{ if } : h \geq a \tag{2}$$

$$\widehat{\gamma}(h) = C_0 + C\left[1 - e^{\left(\frac{h}{a}\right)^2}\right] \tag{3}$$

$$\mathrm{SD} = \frac{C_0}{C_0 + C} \times 100 \tag{4}$$

wherein $\widehat{\gamma}(h)$ = semi variance; C_0 = nugget effect; $C_0 + C$ = threshold; C = contribution; a = reach; and h = distance.

After checking the SDD, the exponential model was used, since it had the lowest values among the models tested; i.e., the data presented the greatest spatial dependence (Fig. 2).

Finally, a grid of 5 × 5 pixels was delimited around the in situ measurement area (micrometeorological tower) and the mean of the LST values contained in this area was extracted for further validation (Fig. 3). The night images corresponding to astronomical days 009, 049, 057, and 353 were excluded from the analysis because

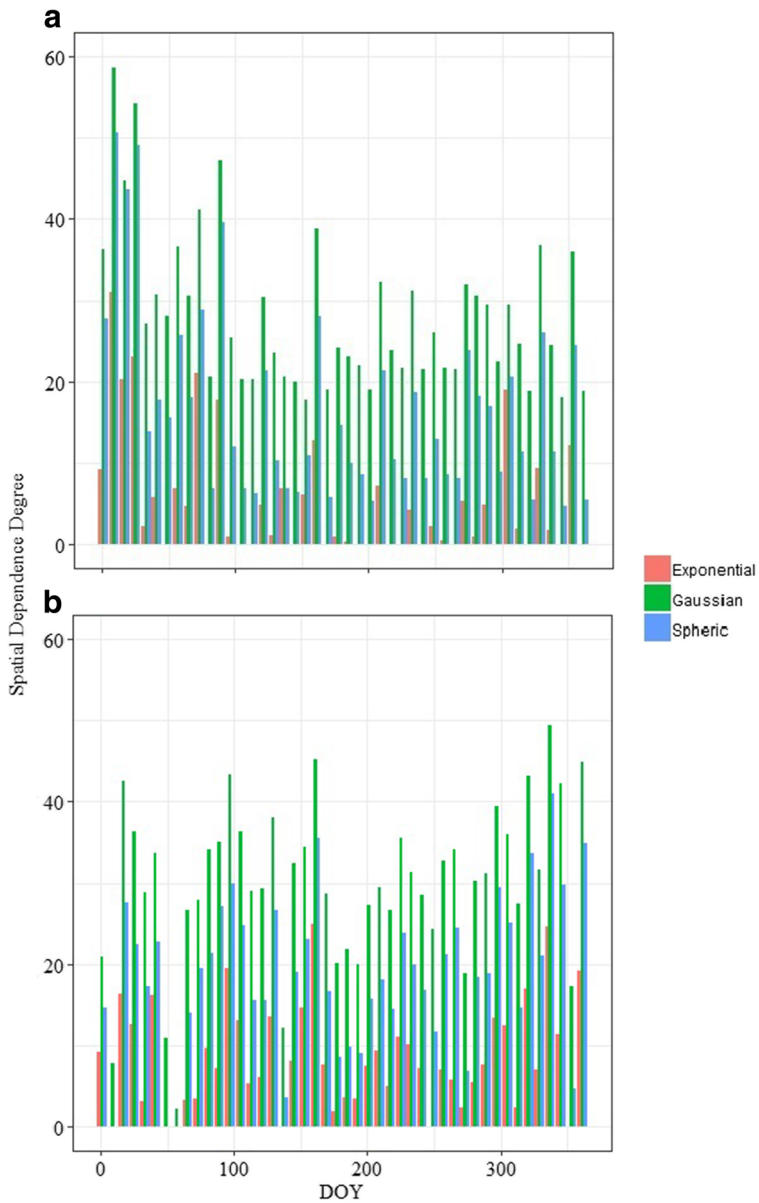

Fig. 2 Spatial dependence degree (GDE) of the **a** daytime and **b** nighttime geostatistical models

of the low number of valid pixels, which impaired the interpolation of the data.

The data from the product MOD11A2 were also used to characterize the land surface temperature of Itatiaia National Park. For this purpose, the monthly average was calculated using the Raster Calculator tool of the ArcGis 10.5 software. Later, the LST data by land use class were extracted using the Zonal Statistics as Table tool. The plantation areas were excluded from this analysis because they comprise only 0.56 km^2 of the total area of the PNI, and it is not possible to extract the LST from it since its total area is smaller than the spatial resolution of the MOD11A2 product, which is 1 km^2.

Canopy temperature

The canopy temperature data were collected by an infrared radiation sensor coupled to the micrometeorological tower located in the lower part of Itatiaia National Park. Installed in 2015 and in operation since 2017, the tower has 30 m height, along which were coupled sensors used in this one and another research. The tower

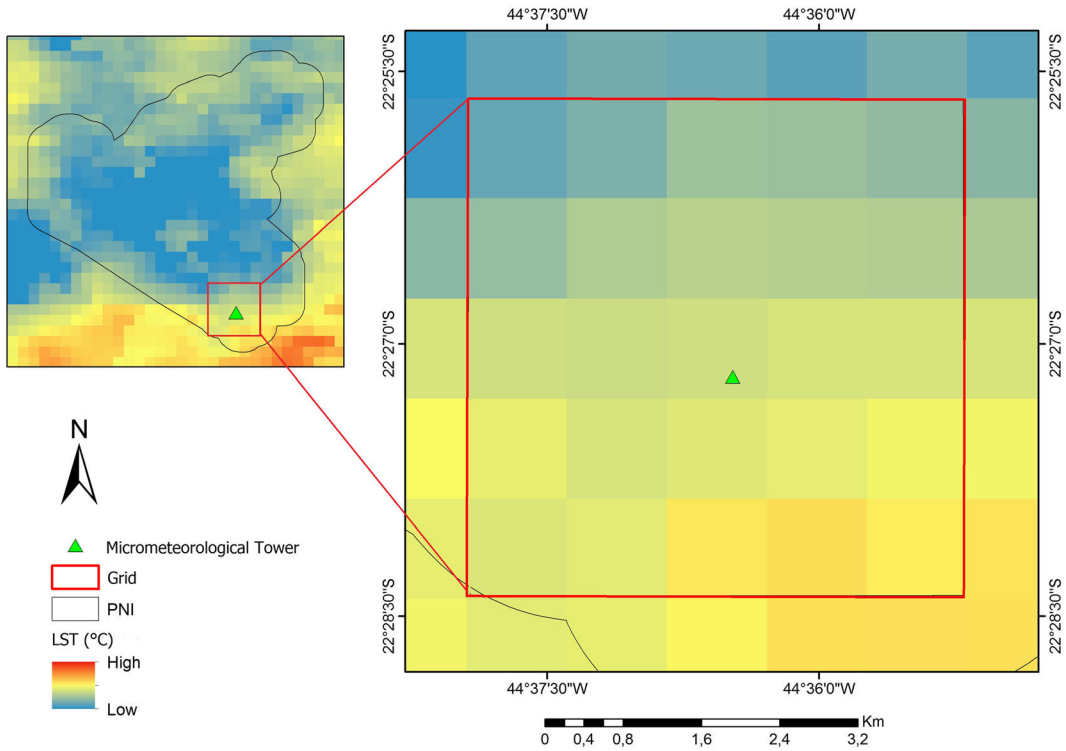

Fig. 3 Delimited area for extraction of LST values

is inserted in an area predominantly of dense montane ombrophylous forest, under the geographical coordinates 22° 27′ 10.83″ S and 44° 36′ 28.51″ W (Fig. 4).

The infrared radiation sensor used was the infrared radiometer model SI-111 from Apogee, installed 27.5 m high, above the nearest vegetation canopy. The device determines the temperature of an object remotely in a passive way by measuring the electromagnetic waves emitted in the infrared range and has a range of up to 1 km. The SI-111 contains a thermopile, which measures the surface temperature, and a thermistor, which measures the temperature of the sensor body. The datalogger uses an equation to correct the effect of sensor body temperature on the target temperature. The corrected readings produce an absolute accuracy of ± 0.2 °C, at temperatures between − 30 and + 65 °C.

The canopy temperature data were collected on an hourly scale, from January 1 to December 31, 2018, totaling 8760 measurements. For the comparison with the orbital data, the temperatures captured close to the times of the satellite passage (approximately 10 h and 23 h) were selected and the average of these observations was performed over an 8-day interval, thus coinciding with the same period of measurements of the MODIS sensor. Thus, for each image from the MODIS sensor, a corresponding canopy temperature value was obtained collected by the infrared radiation sensor installed in the micrometeorological tower.

The characterization of this variable was performed through boxplot produced by the ggplot2 package (WICKHAM 2016) in the R software. The daytime (AM) was considered the interval between 06 and 17 h, and the nighttime (PM) between 18 and 05 h. To indicate the hydric stress of vegetation, the time difference between canopy temperature and the air temperature was calculated and presented through a line graph produced in the software R.

Weather variables

Besides the infrared radiation sensor, the PNI micrometeorological tower also has 5 other sensors (Fig. 5). There are two air temperature and relative humidity measuring sensors model HC2S3 from Campbell Scientific, protected by model 41003 solar radiation shields from Young, positioned at 2 and 10 m high. A Gill WindSonic sensor for wind speed and direction measurements was installed at a height of 10 m. Two sensors

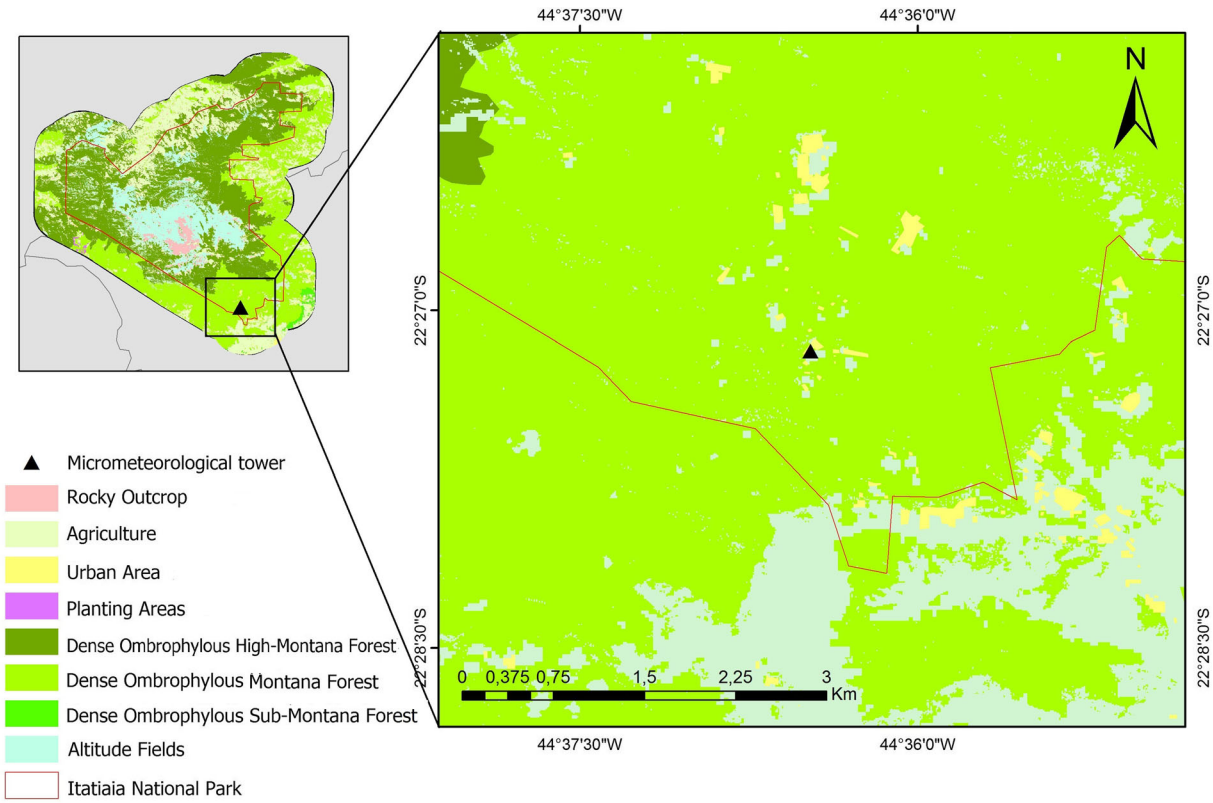

Fig. 4 Geographic location of the micrometeorological tower

model HFP01 from the Hukseflux for measuring the soil heat flux, one buried in a shaded area and the other in full sun. All data collected are stored in the CR3000 datalogger from Campbell Scientific.

For this study, we used air temperature (°C), relative humidity (%), and wind direction (°) and speed (m s^{-1}) data, collected by sensors coupled to the PNI micrometeorological tower. The data were made available on an hourly scale and then converted into daily averages, separated between day and night periods. The temperature and air relative humidity were characterized by boxplot made using the ggplot2 package in the R software. For the wind speed and direction data, the free software WRPLOT VIEW 8.0.2 was used, through which the wind rose was built.

Orbital data validation

For validating the MOD11A2 product, a comparative analysis was performed between the land surface temperature data obtained from the MODIS sensor and the canopy temperature data obtained from the SI-111 infrared radiation sensor. For this purpose, a simple linear regression was applied, using as dependent variable the LST from the MOD11A2 product and the canopy temperature from the SI-111 sensor as independent variable. For a better analysis, data were separated by climate quarters, as follows: January, February, and March (JFM); April, May, and June (AMJ); July, August, and September (JAS); and October, November, and December (OND).

The overall regression model is given by

$$Y = \beta_0 + \beta_1 x + \varepsilon \tag{5}$$

where Y indicates the dependent variable; β_0 is the angular coefficient; β_1 is the linear coefficient; x represents the independent variable, and ε represents the error.

To determine the degree of correlation between the data, the Pearson correlation coefficient (r) was calculated, as expressed by Eq. 6.

$$r = \sqrt{r^2} \tag{6}$$

where r^2 represents the coefficient of determination calculated in linear regression.

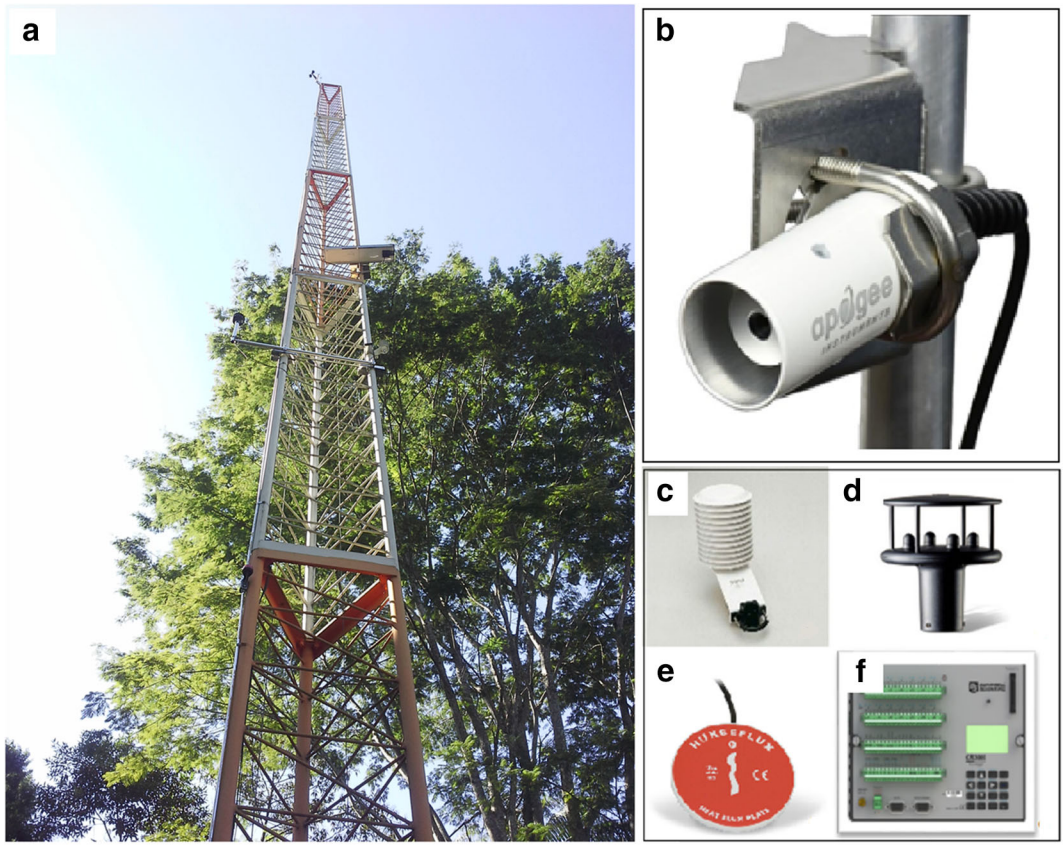

Fig. 5 PNI micrometeorological tower and coupled devices. **a** Tower. **b** Infrared radiation sensor. **c** Air temperature and humidity sensor. **d** Wind sensor. **e** Soil heat flux sensor. **f** Datalogger

The correlation coefficient values found were classified according to Cohen (1988) (Table 2).

The errors associated with the data were evaluated by calculating the mean bias (MB) (Eq. 7) and the root mean square error (RMSE) (Eq. 8).

$$\mathrm{MB} = \frac{1}{N}\sum_{i=1}^{n}\left(X_{\mathrm{ei}} - X_{\mathrm{oi}}\right) \tag{7}$$

$$\mathrm{RMSE} = \left(\frac{1}{N}\sum_{i=1}^{n}\left(X_{\mathrm{ei}} - X_{\mathrm{oi}}\right)^2\right)^{\frac{1}{2}} \tag{8}$$

Finally, the concordance index developed by Willmott (1981) was calculated, which mathematically quantifies the data dispersion in relation to the method considered standard. The Willmott index (d) is expressed by the following equation:

$$d = 1 - \left[\frac{\sum\left(X_{\mathrm{ei}} - X_{\mathrm{oi}}\right)^2}{\sum\left(\left|X_{\mathrm{ei}} - \overline{X_{\mathrm{o}}}\right| + \left|X_{\mathrm{oi}} - \overline{X_{\mathrm{o}}}\right|\right)^2}\right] \tag{9}$$

where X_{ei} represents the estimated data (product MOD11A2) and X_{oi} represents the observed data (canopy temperature collected by the SI-111 sensor).

Table 2 Ranking of Pearson's correlation coefficient values (r)

Correlation coefficient (r)	Ranking
0.0 to 0.1	Very low
0.1 to 0.3	Low
0.3 to 0.5	Moderated
0.5 to 0.7	High
0.7 to 0.9	Very high
0.9 to 1.0	Nearly perfect

Results and discussion

Characterization of variables

Weather variables

The annual average air temperature was 23.23 °C, with an average of 24.40 °C for the daytime and 22.05 °C for the nighttime. Considering the monthly average, the values varied from 21.09 (JUL) to 27.01 °C (DEC) in the daytime period and from 18.70 (JUL) to 23.98 °C (OUT) in the nighttime (Fig. 6). The high temperatures during the day and the low relative humidity of the air contributed for December to present the biggest temperature difference between the day and night periods (3.34 °C).

It can be observed that the air temperature followed the climatic seasonality of the region, presenting lower values in the dry season (April to September) and higher values in the rainy season (October to March). July had the lowest temperatures of the year, mainly influenced by the advance of two cold fronts followed by a strong mass of cold air, which is associated with the pattern of high pressure from surface to medium levels which also favored that this month had the lowest levels of relative humidity of air in the year analyzed (INFOCLIMA 2020).

These differences are in turn associated with geographical factors, vegetation, elevation, and ocean proximity, which causes these fluctuations within the state of Rio de Janeiro to occur (Silva and Dereczynski 2014).

The advance of cold fronts and the location of the high pressure systems positioned in the southeast region also influence the temperature values of the PNI. The entry of cold air masses mainly during the winter influences the temperature drop mainly during this quarter (May, June, and July) throughout Brazil (INFOCLIMA 2020).

The air relative humidity showed an annual average of 88.55%, ranging from 84.62 in July to 91.27% in October (Fig. 6). In the daytime period, the average relative humidity was 84.68%, with the lowest average value observed in September (79.01%) and the highest in June (88.69%), both in the dry periods.

The air relative humidity showed the highest values during the nighttime period, with an annual average of 92.43%. Overall, the monthly nighttime average values were high, ranging from 87.70 in July, dry season, to 94.61% in October, beginning of the rainy season.

Regarding the high mean values of air relative humidity in the PNI in the rainy season, the high relative humidity, associated with intense solar radiation in this period, favors greater absorption of carbon by forests. In a recent study in the PNI evaluating the seasonality of gross primary production (GPP), the authors found higher values of GPP mainly in the rainy season (Delgado et al. 2018).

The high relative humidity found during the rainy season is due to the phenomenon known as the South Atlantic convergence zone (ZACAS), which dynamically influences the rains in the southeast region of Brazil, increasing the cloudiness and relative humidity of the air during the rainy season (INFOCLIMA 2020).

Regarding wind intensity, the monthly average varied from 0.48 (MAR) to 0.72 m s^{-1} (NOV) considering the daytime period. While in the nighttime period, the

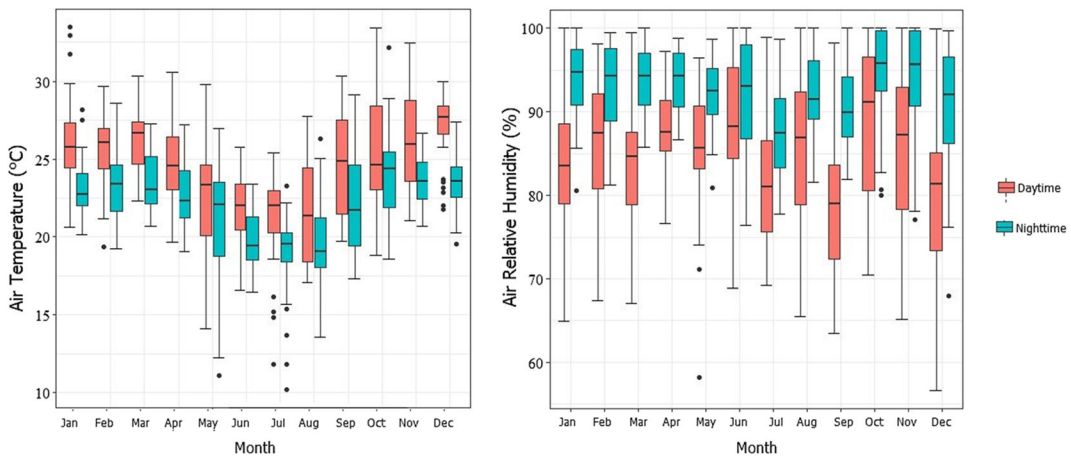

Fig. 6 Boxplot of weather variables air temperature and relative humidity

variation ranged from 0.48 in February to 0.67 m s^{-1} in November. The annual average was in the range of 0.6 m s^{-1} for both periods, classifying its intensity as light air (intensity 1) by Beaufort scale (WMO 2008). Analyzing the wind direction, we notice a higher occurrence in the southeast direction (SE) for the daytime data, signaling the performance of the sea breeze system. For the nighttime period, the predominant direction was northeast (NE), influenced by the mountain-valley breeze system (Fig. 7).

In a recent study in the Serra do Mar region of the state of Rio de Janeiro, the authors associated the predominant speeds and directions with the slopes and oceanic proximity (Sobral et al. 2018). The wind speed in the PNI is influenced by its topography and its proximity to the Atlantic Ocean. Besides the topography, the position of the semi-permanent anticyclone is very active at some times of the year mainly in the winter and spring (INMET 2020), which gradually increases the wind speed and its predominant direction in the PNI.

Canopy temperature

The canopy temperature, collected by the SI-111 infrared radiation sensor, showed an annual average value of 18.42 °C, with an average of 19.74 °C in the daytime period and 17.10 °C in the nighttime period.

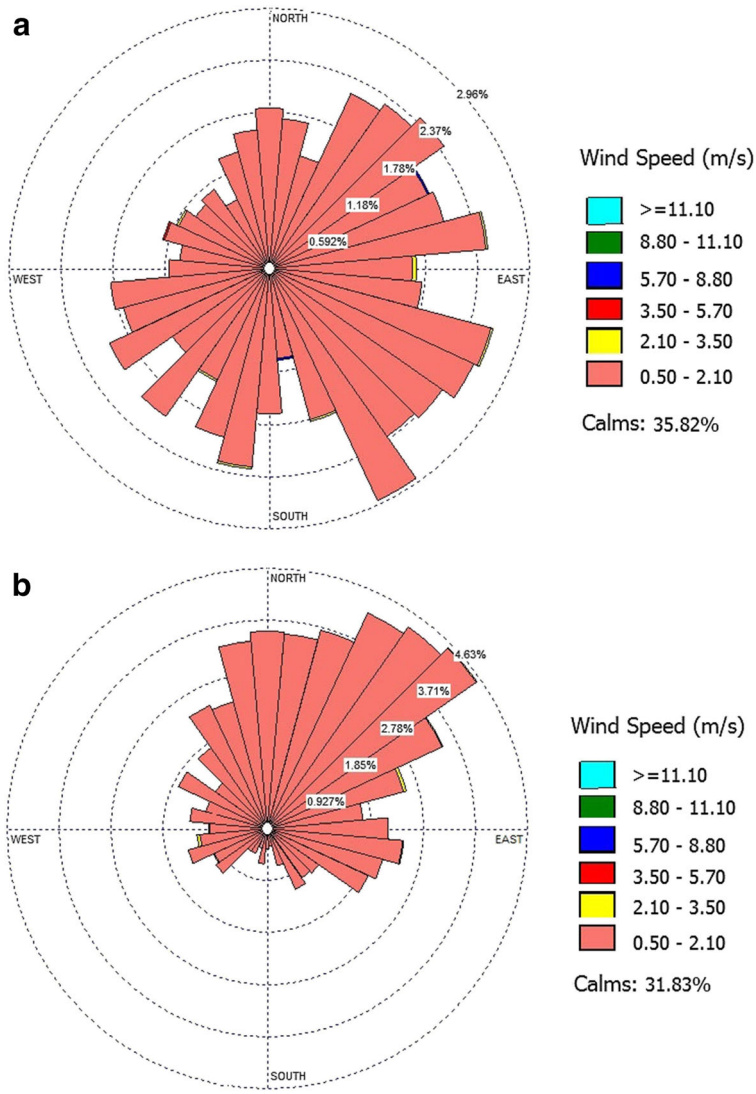

Fig. 7 Wind rose of the micrometeorological station of the PNI for the **a** daytime and **b** nighttime periods

Analyzing the monthly data, the average canopy temperature varied from 16.29 in August to 23.03 °C in December for the daytime period, and from 14.06 in July to 19.70 °C in March for the nighttime period. The variation throughout the year also followed the seasonality of the region, presenting lower values during the dry season and higher values during the rainy season (Fig. 8).

The maximum canopy temperature recorded in 2018 was 31.83 °C, which occurred at 3:00 pm on December 18. Some researches carried out in tropical forests showed that the optimal temperature of photosynthesis occurs between 20 and 36 °C, indicating that when the leaf temperature values exceed this range, the process of carbon fixation by the plant starts to decrease (Graham et al. 2003; Tribusy 2005; Felsemburgh 2009). In the PNI, the forest canopy temperature remained within the optimal temperature range for photosynthesis at 30.48% of the time in the analyzed period.

The lowest recorded canopy temperature was 5.21 °C, which occurred at 07:00 am on July 12th. This date presented the lowest daily average of the year for this variable, with 9.10 °C. The highest daily average of the canopy temperature was 25.09 °C, on December 18.

In Fig. 9, it is possible to observe the variation of the canopy temperature throughout the day and make a comparison with the other variables collected by the PNI micrometeorological tower. The canopy temperature has an increasing behavior from 6:00 am, reaching its maximum point at 3:00 pm. The canopy temperature follows a daytime curve, with temperatures rising due to increased solar radiation and air temperature. In periods of higher values of the canopy temperature, the local condition found was high air temperature and low relative humidity and wind speed.

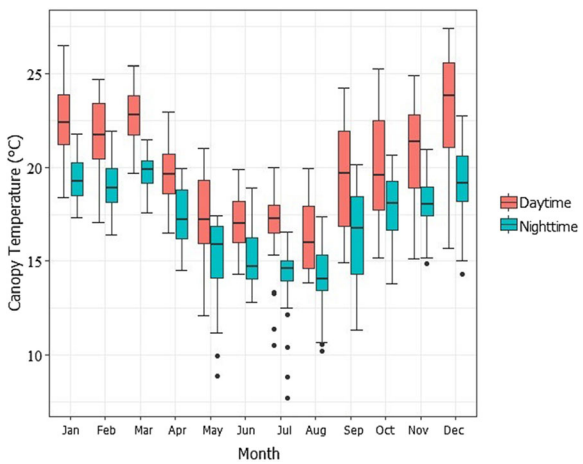

Fig. 8 Boxplot of monthly canopy temperature

The canopy temperature was on average 4.76 °C below the air temperature. Under normal conditions, the canopies have a temperature close to the air, warming significantly under conditions of water restriction (Scherrer et al. 2011). Thus, the average difference between canopy temperature and air temperature can be used as an indicator of plant water stress (Dejonge et al. 2015; Duffková 2006; Keener and Kircher 1983). The negative result shown in Fig. 10 indicates that the potential for hydric stress in the studied area is minimal.

Land surface temperature

Land surface temperature (LST) in the Itatiaia National Park presented an annual average of 20.26 °C during daytime and 12.26 °C during nighttime. As shown in Fig. 11, the highest temperatures occurred in the southern part of the park, corresponding to the lower portion of the PNI, which shows the altitude effect on the LST result. Khandan et al. (2018), in a study on maximum surface temperature in Iran, observed that NDVI (Normalized Difference Vegetation Index) and altitude had the highest correlations with the observed LST.

May, June, and July were the months with the lowest mean values of LST in both periods, 17.30 °C, 17.39 °C, and 17.24 °C during daytime and 10.23 °C, 10.26 °C, and 10.58 °C during nighttime (Table 3 and Fig. 11).

The highest mean LST was in December, with 23.26 °C in the daytime period, while in the nocturnal period, the month of March presented the highest mean, with 14.91 °C. The difference between day and night temperatures was more pronounced in November, where the daytime average was 21.77 °C and the nighttime average was 10.64 °C. The high data dispersion is justified by the great heterogeneity of the park's landscape, which has 8 different land use and land cover, and high altitudinal amplitude.

The LST by land use and coverage was analyzed considering 7 of the 8 classes identified in the park, excluding the planting areas from this analysis because they have a total area smaller than the minimum area captured by the sensor (Table 4 and Fig. 12).

The altitude fields and rocky outcrops presented the lowest LST values, which were respectively 17.74 °C and 18.12 °C in the daytime period and 9.29 °C and 9.10 °C in the nighttime period. These classes occur at the top

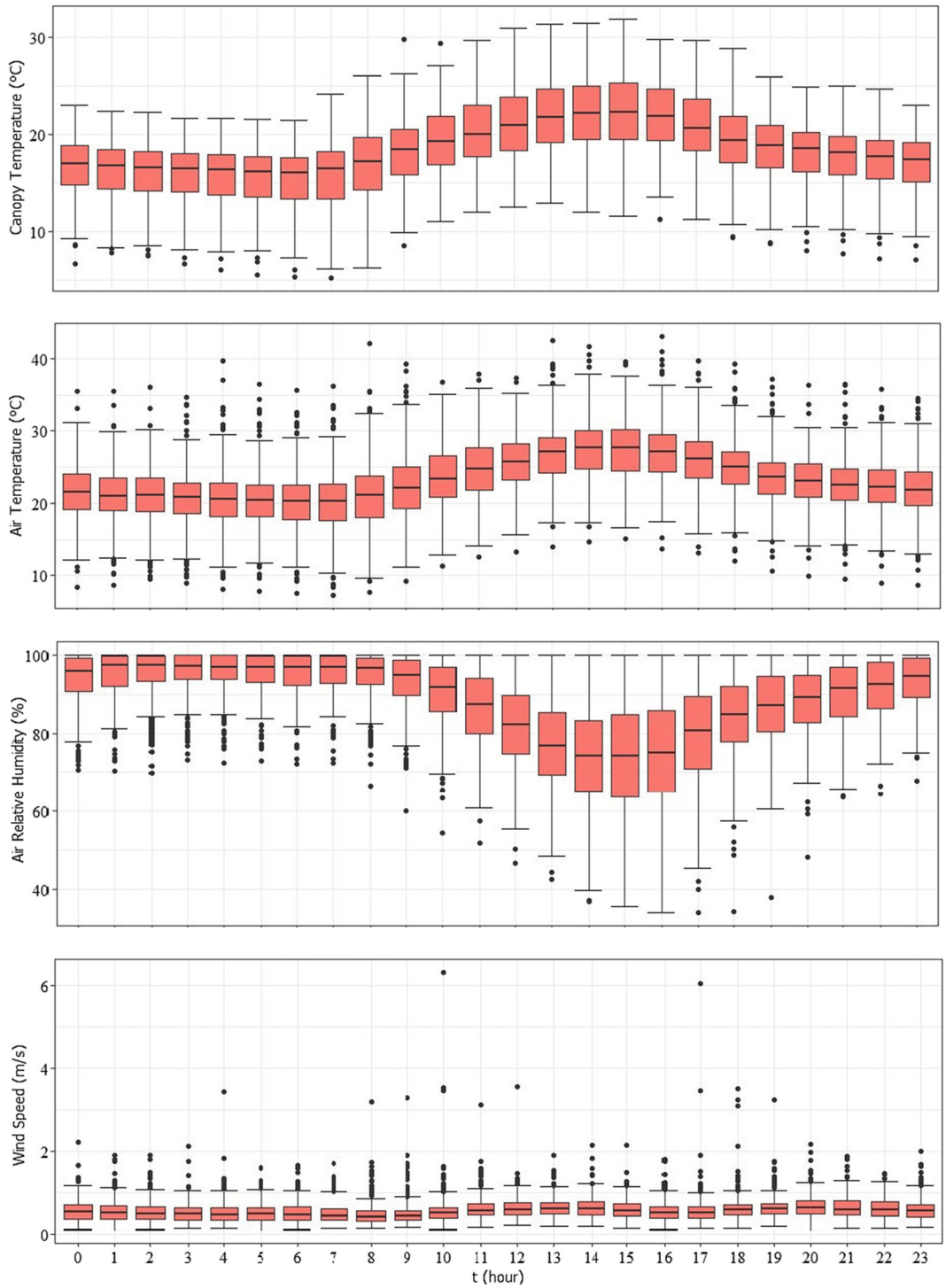

Fig. 9 Hourly variation of micrometeorological variables

of the PNI mountains, where temperatures below 0 °C and frosts are not so rare (Aximoff et al. 2016; Matos and Rosado 2019).

The highest LST values were observed in the dense ombrophilous sub-montane forest and urban area classes. Overall, the surface temperature in urbanized areas

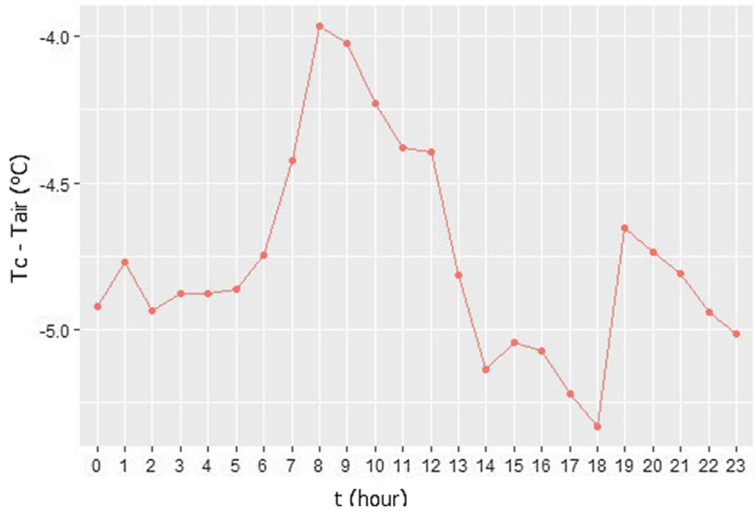

Fig. 10 Difference between canopy temperature (T_c) and air temperature (T_{air})

tends to be higher than in natural areas (Han and Xu 2013; Madanian et al. 2018). The surfaces found in these areas are mostly impermeable, and materials with this characteristic have a high capacity to store energy and generate higher temperatures (Moghbel and Shamsipour 2019). According to Imhoff et al. (2010), the impermeable surface area is the main responsible for increased LST in the cities.

The high temperatures found in the dense ombrophilous sub-montane forest class can be explained by its geographical location, with the entire area concentrated in the lower part of the park. The differences in LSTs of the three forest classes show the altitude effect on the surface temperature, since the high montane class, which occurs in areas above 2000 m in altitude, presented the lowest average between the three classes in both periods (19.09 °C and 11.47 °C), followed by the montane class (21.66 °C and 14.18 °C) and finally the sub-montane class (24.95 °C and 16.21 °C).

Overall, the average values of LST were lower in the dry season for all classes of land use and land cover in both periods, although the classes urban area, dense ombrophilous montane forest, and dense ombrophilous sub-montane forest present the lowest monthly average in November during the nighttime.

Orbital data validation

Figure 13 presents the monthly behavior of the observed (SI-111) and estimated (MOD11A2) canopy temperature for the year 2018 in the PNI. We observed that in both periods, the temperature follows the seasonality of the region, presenting lower values in the dry season (April to September) and higher values in the rainy season (October to March). A more atypical behavior was observed for the LST in November during the nighttime, where the temperature estimated by the MO11A2 product presented the lowest average of the year.

For the daytime period, the estimated LST data were larger than the data collected by the SI-111 sensor, while in the nighttime period, the opposite behavior was found. The mean bias (MB) values (Table 5) confirm the tendency of the MOD11A2 product to overestimate the canopy temperature in the daytime period (positive values ranging from 1.56 to 3.57 °C) and underestimate in the nighttime period (negative values ranging from − 0.18 to − 4.22 °C). A similar result to that found here was observed by Gomis-Cebolla et al. (2018), where daytime surface temperature data from the MODIS sensor overestimated the canopy temperature in a dense forest area in Peruvian Amazonia, showing an MB value above 3 °C.

The canopy temperature was estimated more accurately in the daytime period, where the highest values of Pearson's correlation index and Willmott index were found (Table 5). The quarters corresponding to the dry season presented a very high correlation between the estimated and observed data, whose values were 0.74 for April to June and 0.86 for July to September. This same period also presented the highest values of the Willmott index (0.70 and 0.64, respectively).

In the nighttime period, the MOD11A2 product did not present a good performance for estimating the LST

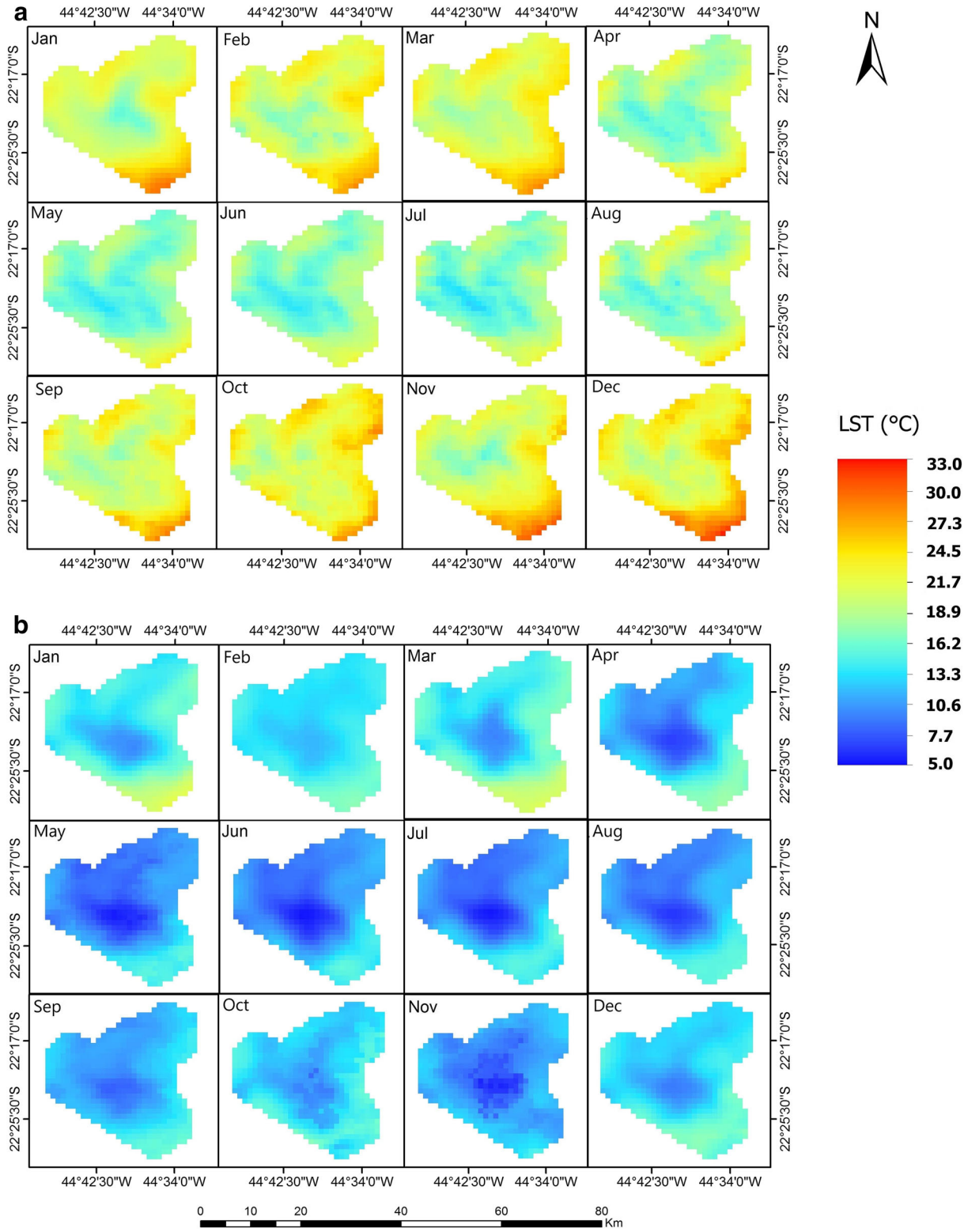

Fig. 11 Monthly variation of LST **a** daytime and **b** nighttime

Table 3 Descriptive statistics of the monthly LST

Period		Jan	Feb	Mar	Apr	May	Jun	Jul	Aug	Sep	Oct	Nov	Dec
Daytime	Min	15.61	16.77	17.61	14.67	13.41	13.55	12.61	14.20	16.97	17.82	15.43	18.38
	Max	29.90	28.71	28.89	26.19	23.90	22.63	22.70	25.45	28.96	28.59	30.99	32.49
	Mean	21.37	21.50	21.99	18.88	17.30	17.39	17.24	18.54	21.32	22.58	21.77	23.26
	Deviation	2.56	2.40	2.19	2.31	2.00	1.84	1.95	2.07	2.29	2.10	2.92	2.66
	CV%	11.98	11.17	9.95	12.23	11.55	10.56	11.31	11.14	10.74	9.31	13.43	11.43
Nighttime	Min	9.89	9.56	9.59	6.85	5.52	5.31	5.43	6.49	8.07	8.45	5.83	9.20
	Max	21.97	22.23	21.27	17.91	15.43	15.53	16.04	15.82	16.15	17.14	14.76	17.16
	Mean	14.77	14.54	14.91	12.04	10.23	10.26	10.58	10.95	11.87	12.93	10.64	13.42
	Deviation	2.42	2.71	2.58	2.62	2.26	2.23	2.38	2.27	1.76	1.62	1.69	1.84
	CV%	16.38	18.64	17.30	21.76	22.09	21.73	22.50	20.73	14.83	12.53	15.88	13.71

of the PNI, mainly in the rainy period, presenting a negative correlation and low index of agreement in January to March (− 0.51 and 0.11) and October to December (− 0.07 and 0.18). However, the lowest value of RMSE found in this analysis was observed during the rainy season (1.58 °C in the quarter January to March). Despite the low value of the error, the results of Pearson's correlation and Willmott index point out the insufficient performance of the LST estimate for this period. For the dry period, the correlation was very low for July to September (0.05) and moderate for April to June (0.43), with Willmott index ranging from 0.46 to 0.51 and RMSE from 2.19 to 2.48 °C, respectively.

The surface temperature dispersion observed by the SI-111 sensor and estimated by the MOD11A2 product for the daytime and nighttime periods can be seen in Fig. 14.

Overall, the months corresponding to the rainy season had a lower performance, in which the worst LST estimate occurred in October to December in both periods, where low correlations between observed and estimated data (0.11 and − 0.07), high RMSE (5.06 °C and 5.00 °C), and low Willmott index (0.41 and 0.18) were found.

Through the quality control analysis of the images used, we observed that the daytime images in the sampled area presented 20.06% more pixels with good quality compared to the nighttime images. Likewise, the images from the months corresponding to the dry period presented 25.57% more pixels with good quality compared to the images corresponding to the rainy season (Fig. 15).

Thus, it is possible to affirm that the MOD11A2 product presented a lower efficiency in humid

Table 4 Descriptive statistics of LST by class and land use. (A) Rocky outcrop, (B) agriculture, (C) urban area, (D) high altitude fields, (E) planting areas, (F) dense ombrophylous high montane forest, (G) dense ombrophylous montane forest, and (H) dense ombrophylous sub-montane forest

Period		A	B	C	D	F	G	H
Daytime	Min	15.08	18.21	20.10	14.93	16.21	18.48	20.56
	Max	21.24	24.28	27.59	20.74	21.83	25.13	29.34
	Mean	18.12	21.31	23.82	17.74	19.07	21.66	24.95
	STD	2.32	2.20	2.73	2.12	2.12	2.44	2.92
	CV%	12.78	10.34	11.48	11.95	11.11	11.25	11.71
Nighttime	Min	6.74	10.30	11.72	7.10	9.43	11.91	11.93
	Max	11.25	15.33	18.11	11.49	13.92	17.14	20.44
	Mean	9.10	12.43	14.69	9.29	11.47	14.18	16.21
	STD	1.74	1.95	2.17	1.71	1.71	1.88	2.78
	CV%	19.15	15.72	14.78	18.42	14.90	13.24	17.17

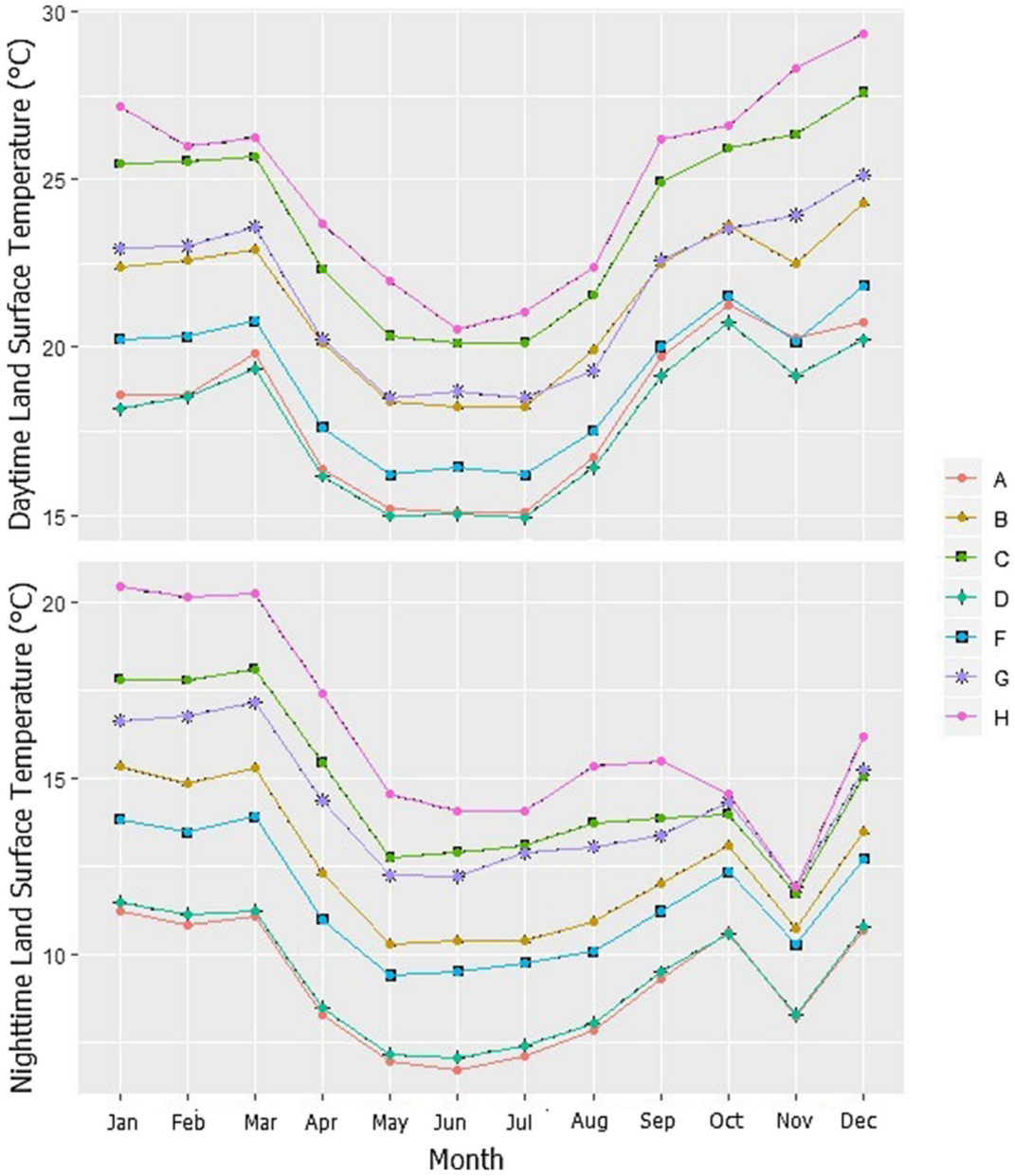

Fig. 12 Land surface temperature by land use and land cover. (**A**) Rocky outcrop, (**B**) agriculture, (**C**) urban area, (**D**) high altitude fields, (**E**) planting areas, (**F**) dense ombrophylous high montane forest, (**G**) dense ombrophylous montane forest, and (**H**) dense ombrophylous sub-montane forest

atmospheric conditions, where the greater quantity of good quality pixels directly interfered in the LST estimate. The interference of the amount of atmospheric water vapor in the LST estimation by remote sensing was also reported by other authors (Coll et al. 2009; Li et al. 2014).

It is important to highlight that spatially heterogeneous areas are not suitable for validating orbital surface temperature data, especially those with a spatial resolution of 1 km or more (Coll et al. 2009). These areas present great spatial variability of LST, which interferes with the assessment results. However, it is necessary to validate these data in different land use and land cover classes, as in the Atlantic Forest area used here, aiming at inferring on the applicability of these products in different environments.

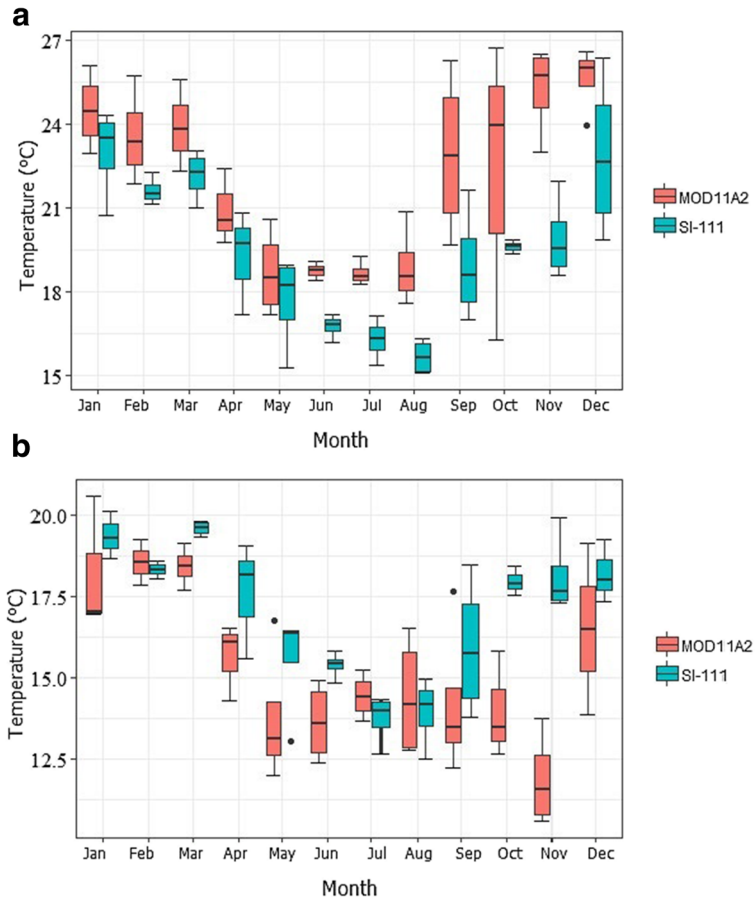

Fig. 13 Boxplot of monthly LST derived from SI-111 sensor and MOD11A2 product. **a** Daytime. **b** Nighttime

Conclusions

The variation in the monthly air temperature and canopy patterns collected by the instruments coupled to the PNI micrometeorological tower characterizes well the distinction between the rainy and dry periods. However, the air relative humidity is high at all times of the year, mainly during the night period.

The land surface temperature is higher in the lower part of the Itatiaia National Park, which highlighted the

Table 5 Statistical analysis between the canopy temperature collected by the SI-111 sensor and the LST estimated by the MOD11A2 product for the year 2018 in PNI

Period	Quarter	*N*	*r*	MB (°C)	RMSE (°C)	*d*
Daytime	JFM	12	0.52	1.74	2.12	0.56
	AMJ	11	0.74	1.56	1.90	0.70
	JAS	12	0.86	3.18	3.46	0.64
	OND	11	0.11	3.67	5.06	0.41
Nighttime	JFM	9	− 0.51	− 0.85	1.58	0.11
	AMJ	11	0.43	− 1.83	2.48	0.51
	JAS	12	0.05	− 0.18	2.19	0.46
	OND	10	− 0.07	− 4.22	5.00	0.18

N sample size; *r* Pearson's correlation coefficient; *MB* mean bias; *RMSE* root mean square error; *d* Willmott index

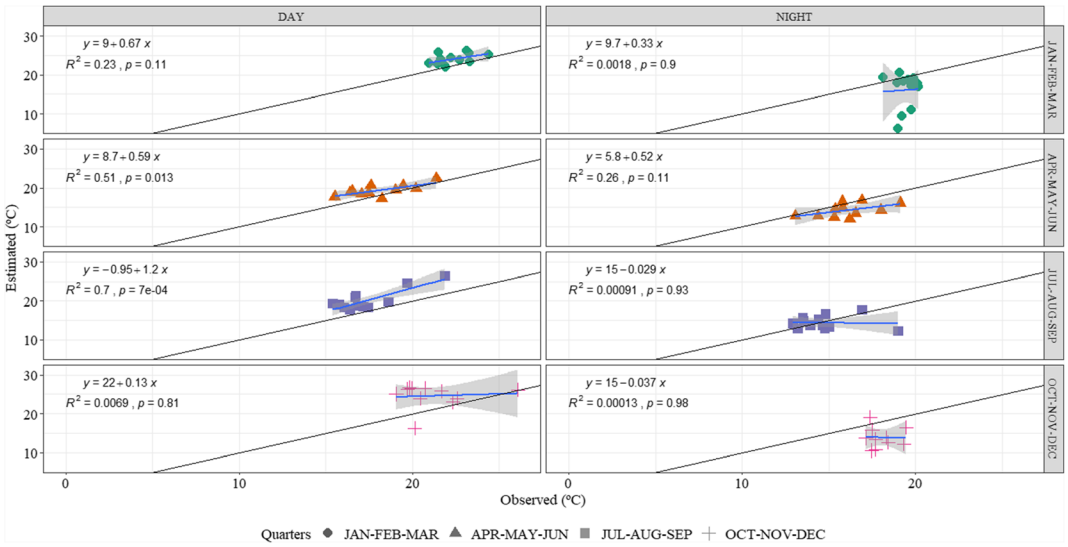

Fig. 14 Dispersion of day and night data observed by the SI-111 sensor as a function of those estimated by the MOD11A2 product

altitude effect on LST values. The lowest LST values in the PNI are observed in May, June, and July, both during the day and night.

Among the forms of land use and land occupation classified in the PNI, the altitude fields and rocky outcrops have the lowest LST values. The highest values are observed in areas of dense ombrophilous submontane forest and urban area.

The canopy temperature is overestimated by the MOD11A2 product in the daytime period and underestimated in the nighttime period. MOD11A2 presents a better estimation of the canopy temperature during the day and months corresponding to the dry season, indicating that this product has limitations to estimate the surface temperature in high humidity atmospheric conditions.

The use of remote sensing to estimate TST in the PNI can assist in understanding the dynamics of the park's vegetation, facilitating the identification of its vulnerabilities and decision-making. It can be used, for example, to recognize times of the year, areas, and

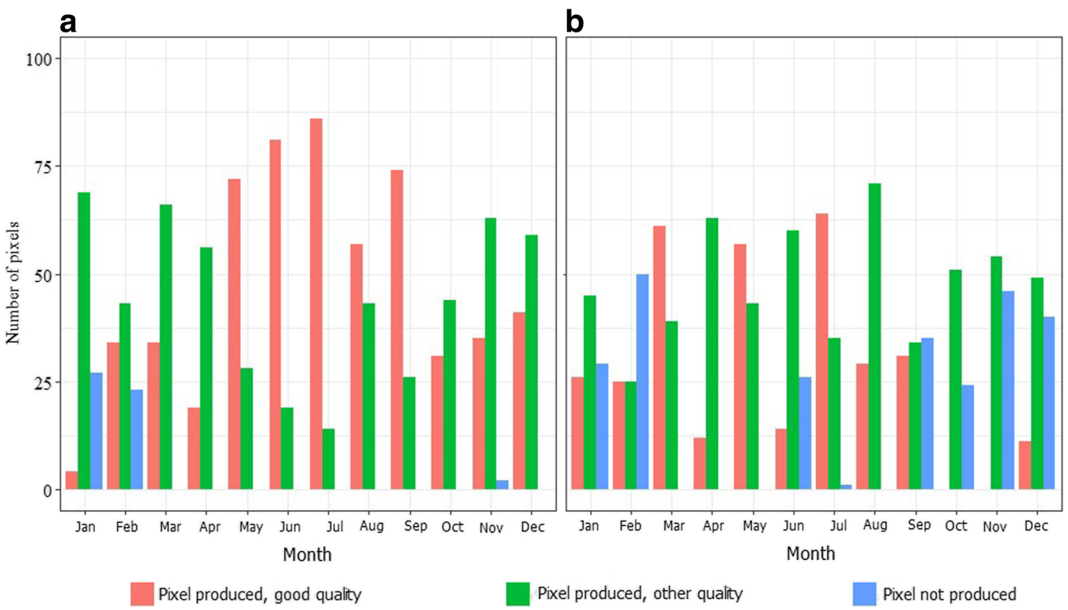

Fig. 15 Quality of the sample pixels for the **a** daytime and **b** nighttime periods

phytophysiognomies most susceptible to the occurrence of forest fires. From these orbital data, which are made available daily and free of charge, environmental monitoring becomes more efficient and assertive, proving to be an important tool for the management of conservation units and green areas.

Finally, we highlight that the results presented in this paper refer to an Atlantic Forest area, with specific land cover and atmospheric conditions. Therefore, to evaluate the applicability of the MOD11A2 product in other environments, additional studies in sites and atmospheric conditions different from those presented here are necessary.

Acknowledgments We would like to thank the Chico Mendes Institute for Biodiversity Conservation and all the employees at Itatiaia National Park, Rio de Janeiro who somehow helped with the research. We would also like to thank the National Aeronautics and Space Administration (NASA) for the availability of free MODIS sensor images.

Funding The authors received financial support from the Research Support Foundation of the State of Rio de Janeiro - FAPERJ (No. 203.152/2017) and the National Council for Scientific and Technological Development - CNPq (No. 304966/2017-7).

References

Alvares, C. A., Stape, J. L., Sentelhas, P. C., De Moraes Gonçalves, J. L., & Sparovek, G. (2013). Köppen's climate classification map for Brazil. *Meteorologische Zeitschrift, 22*(6), 711–728. https://doi.org/10.1127/0941-2948/2013/0507.

APOGEE. (2018). No Title. https://www.apogeeinstruments.com/infraredradiometer/. Accessed 15 July 2018

Aximoff, I., Nunes-Freitas, A. F., & Braga, J. M. A. (2016). Regeneração natural pós-fogo nos campos de altitude no Parque Nacional do Itatiaia , Sudeste do Brasil. *Oecologia Australis, 20*(2), 62–80. https://doi.org/10.4257/oeco.2016.2002.05.

Barreto, C.G., Campos, J.B., Roberto, D.M., Roberto, D.M., Teixeira, N., Alves, G.S.G., Coelho, W. (2013). Plano de manejo Parque Nacional do Itatiaia. http://www.icmbio.gov.br/portal/images/stories/docs-planos-de-manejo/pm_parna_itatiaia_enc1.pdf. Accessed 15 July 2018

Busetto, L., & Ranghetti, L. (2016). MODIStsp : an R package for automatic preprocessing of MODIS Land Products time series. *Computers and Geosciences, 97*, 40–48. https://doi.org/10.1016/j.cageo.2016.08.020.

Cambardella, C. A., Moorman, J. M., Novak, T. B., Parkin, D. L., Karlen, R. F. T., & Konopka, A. E. (1994). Field-scale variability of soil properties in Central Iowa soils. *Soil Sciety of America Journal, 58*, 1501–1511.

Çamoğlu, G. (2013). The effects of water stress on evapotranspiration and leaf temperatures of two olive (Olea europaea L.) cultivars. *Zemdirbyste-Agriculture, 100*(1), 91–98. https://doi.org/10.13080/z-a.2013.100.012.

Cohen, J. (1988). Statistical power analysis for the behavioral sciences, 2nd edn. Á/L.

Colaizzi, P. D., O'Shaughnessy, S. A., Evett, S. R., & Mounce, R. B. (2017). Crop evapotranspiration calculation using infrared thermometers aboard center pivots. *Agricultural Water Management, 187*, 173–189. https://doi.org/10.1016/j.agwat.2017.03.016.

Coll, C., Wan, Z., & Galve, J. M. (2009). Temperature-based and radiance-based validations of the V5 MODIS land surface temperature product. *Journal of Geophysical Research, 114*, 1–15. https://doi.org/10.1029/2009JD012038.

Dejonge, K. C., Taghvaeian, S., Trout, T. J., & Comas, L. H. (2015). Comparison of canopy temperature-based water stress indices for maize. *Agricultural Water Management, 156*, 51–62. https://doi.org/10.1016/j.agwat.2015.03.023.

Delgado, R. C., Pereira, M. G., Teodoro, P. E., dos Santos, G. L., de Carvalho, D. C., Magistrali, I. C., & Vilanova, R. S. (2018). Seasonality of gross primary production in the Atlantic Forest of Brazil. *Global Ecology and Conservation, 14*, e00392. https://doi.org/10.1016/J.GECCO.2018.E00392.

Dixon, R. K., Brown, S., Houghton, R. A., Solomon, A. M., Trexler, M. C., & Wisniewski, J. (1994). Carbon pools and flux of global forest ecosystems. *Science, 263*(5144), 185–190. https://doi.org/10.1126/science.263.5144.185.

Duffková, R. (2006). Difference in canopy and air temperature as an indicator of grassland water stress. *soil & Water Res.*, *1*(4), 127–138.

Felsemburgh, C. A. (2009). *Respostas fotossintéticas à variação da temperatura foliar do dossel na flona do Tapajós - PA*. Escola Superior de Agricultura "Luiz de Queiroz", Tese de Doutorado. Universidade de São Paulo. https://doi.org/10.11606/T.91.2009.tde-14092009-082158.

Gomis-Cebolla, J., Jimenez, J. C., & Sobrino, J. A. (2018). LST retrieval algorithm adapted to the Amazon evergreen forests using MODIS data. *Remote Sensing of Environment, 204*(November 2017), 401–411. https://doi.org/10.1016/j.rse.2017.10.015.

Graham, E. A., Mulkey, S. S., Kitajima, K., Phillips, N. G., Graham, E. A., Mulkey, S. S., et al. (2003). Cloud cover limits net CO2 uptake and growth of a rainforest tree during tropical rainy seasons. *Proceedings of the National Academy of Sciences of the United States of America, 100*(2), 572–576.

Gray, S. B., Dermody, O., Klein, S. P., Locke, A. M., McGrath, J. M., Paul, R. E., Rosenthal, D. M., Ruiz-Vera, U. M., Siebers, M. H., Strellner, R., Ainsworth, E. A., Bernacchi, C. J., Long, S. P., Ort, D. R., & Leakey, A. D. B. (2016). Intensifying drought eliminates the expected benefits of elevated carbon dioxide for soybean. *Nature Plants, 2*(9), 1–8. https://doi.org/10.1038/nplants.2016.132.

Guillevic, P. C., Privette, J. L., Coudert, B., Palecki, M. A., Demarty, J., Ottlé, C., & Augustine, J. A. (2012). Land surface temperature product validation using NOAA's surface climate observation networks-scaling methodology for the visible infrared imager radiometer suite (VIIRS). *Remote Sensing of Environment, 124*, 282–298. https://doi.org/10.1016/j.rse.2012.05.004.

Han, G., & Xu, J. (2013). Land surface phenology and land surface temperature changes along an urban–rural gradient in Yangtze River Delta, China. *Environmental Management, 52*, 234–249. https://doi.org/10.1007/s00267-013-0097-6.

Heft-Neal, S., Lobell, D. B., & Burke, M. (2017). Using remotely sensed temperature to estimate climate response functions. *Environmental Research Letters, 12*(1), 014013. https://doi.org/10.1088/1748-9326/aa5463.

Helliker, B. R., Song, X., Goulden, M. L., Clark, K., Bolstad, P., & Munger, J. W. (2018). Assessing the interplay between canopy energy balance and photosynthesis with cellulose δ 18 O: large-scale patterns and independent ground-truthing. *Oecologia, 187*(4), 995–1007. https://doi.org/10.1007/s00442-018-4198-z.

Hiparc. (2011). Projeto IKONOS – Itatiaia. Processamento Digital de Imagens. *Relatório Técnico*, p. 36. Accessed in: 30 Setembro 2020. https://www.icmbio.gov.br/parnaitatiaia/images/stories/boletins_de_pesquisa/bpni_v15_2.pdf.

Hulley, G. C., Hughes, C. G., & Hook, S. J. (2012). Quantifying uncertainties in land surface temperature and emissivity retrievals from ASTER and MODIS thermal infrared data. *Journal of Geophysical Research-Atmospheres, 117*(23), 1–18. https://doi.org/10.1029/2012JD018506.

Imhoff, M. L., Zhang, P., Wolfe, R. E., & Bounoua, L. (2010). Remote sensing of environment remote sensing of the urban heat island effect across biomes in the continental USA. *Remote Sensing of Environment, 114*(3), 504–513. https://doi.org/10.1016/j.rse.2009.10.008.

INFOCLIMA, CLIMATOLOGIA TRIMESTRAL. Accessed in: 30 Setembro 2020. http://infoclima.cptec.inpe.br/.

INSTITUTO BRASILEIRO DE GEOGRAFIA E ESTATÍSTICA - IBGE. (2012). Manual técnico da vegetação brasileira: sistema fitogeográfico, inventário das formações florestais e campestres, técnicas e manejo de coleções botânicas, procedimentos para mapeamentos. *IBGE*, 271. Accessed in: 30 Setembro 2020. http://www.terrabrasilis.org.br/ecotecadigital/pdf/manual-tecnico-da-vegetacao-brasileira.pdf.

INSTITUTO NACIONAL DE METEOROLOGIA - INMET. (2020). Notas Técnicas Climatológicas. http://www.inmet.gov.br/portal/index.php?r=home/page&page=notas_tecnicas. Accessed 20 July 2020.

Keener, M. E., & Kircher, P. L. (1983). The use of canopy temperature as an indicator of drought stress in humid regions. *Agricultural Meteorology, 28*, 339–349.

Khandan, R., Gholamnia, M., Bo, S., Mehrnoosh, D., Seyed, G., & Alavipanah, K. (2018). Characterization of maximum land surface temperatures in 16 years from MODIS in Iran. *Environmental Earth Sciences, 77*(450). https://doi.org/10.1007/s12665-018-7623-z.

Kim, Y., Still, C. J., Hanson, C. V., Kwon, H., Greer, B. T., & Law, B. E. (2016). Canopy skin temperature variations in relation to climate, soil temperature, and carbon flux at a ponderosa pine forest in central Oregon. *Agricultural and Forest Meteorology, 226–227*(August), 161–173. https://doi.org/10.1016/j.agrformet.2016.06.001.

Li, H., Sun, D., Yu, Y., Wang, H., Liu, Y., Liu, Q., du, Y., Wang, H., & Cao, B. (2014). Evaluation of the VIIRS and MODIS LST products in an arid area of Northwest China. *Remote Sensing of Environment, 142*, 111–121. https://doi.org/10.1016/j.rse.2013.11.014.

Madanian, M., Soffianian, A. R., Koupai, S. S., Pourmanafi, S., & Momeni, M. (2018). Analyzing the effects of urban expansion on land surface temperature patterns by landscape metrics: a case study of Isfahan city, Iran. *Environmental Monitoring and Assessment, 190*(189), 189.

Matos, I. S., & Rosado, B. H. P. (2019). Como as plantas dos campos de altitude enfrentam a seca? Desvendando a importância da diversidade funcional e dos eventos de neblina *Boletim do Parque Nacional do Itatiaia*, *30*. Accessed in: 30 Setembro 2020. https://www.icmbio.gov.br/parnaitatiaia/images/stories/boletins_de_pesquisa/bpni_v30.pdf.

Moghbel, M., & Shamsipour, A. A. (2019). Spatiotemporal characteristics of urban land surface temperature and UHI formation: a case study of Tehran. *Iran, 137*(3–4), 2463–2476.

Pérez-díaz, C. L., Lakhankar, T., Romanov, P., Muñoz, J., Lakhankar, T., Romanov, P., & Muñoz, J. (2017). Evaluation of MODIS land surface temperature with in-situ snow surface temperature from CREST-SAFE. *International Journal of Remote Sensing, 38*(15–16), 4722–4740. https://doi.org/10.1080/01431161.2017.1331055.

Scherrer, D., Bader, M. K., & Körner, C. (2011). Drought-sensitivity ranking of deciduous tree species based on thermal imaging of forest canopies. *Agricultural and Forest Meteorology, 151*(12), 1632–1640. https://doi.org/10.1016/j.agrformet.2011.06.019.

Silva, W. L., & Dereczynski, C. P. (2014). Caracterização climatológica e tendências observadas em extremos climáticos no estado do Rio de janeiro. *Anuário do Instituto de Geociências, 37*(2), 123–138. https://doi.org/10.11137/2014_2_123_138.

Sobral, B. S., de Oliveira Júnior, J. F., de Gois, G., Terassi, P. M. d. B., & Pereira, C. R. (2018). Wind regime in Serra do Mar Ridge-Rio de Janeiro, Brazil. *Revista Brasileira de Meteorologia, 33*(3), 441–451. https://doi.org/10.1590/0102-7786333004.

Song, Q. H., Deng, Y., Zhang, Y. P., Deng, X. B., Lin, Y. X., Zhou, L. G., et al. (2017). Comparison of infrared canopy temperature in a rubber plantation and tropical rain forest. *International Journal of Biometeorology, 61*(10), 1885–1892. https://doi.org/10.1007/s00484-017-1375-4.

Tribusy, E. S. (2005). *Variações da temperatura foliar do dossel e o seu efeito na taxa assimilatória de CO2 na Amazônia Central*. Escola Superior de Agricultura "Luiz de Queiroz", Tese de Doutorado. Universidade de São Paulo. https:/doi.org/10.11606/T.91.2005.tde-15072005-144011.

Wan, Z. (2006). *MODIS land surface temperature products users' guide*. University of California, Santa Barbara, CA. Accessed in: 30 Setembro 2020. Retrieved from http://www.oalib.com/references/9184061.

Wan, Z. (2013). MODIS land surface temperature products users' guide. https://icess.eri.ucsb.edu/modis/LstUsrGuide/usrguide.html. Accessed 15 September 2019

Wickham, H. (2016). *ggplot2: elegant graphics for data analysis*. New York: Springer.

Willmott, C. J. (1981). On the validation of models. *Physical Geography, 2*, 184–194.

WMO. (2008). *Guide to meteorological instruments and methods of observation*. Geneva. Accessed in: 30 Setembro 2020. https://www.wmo.int/pages/prog/www/IMOP/CIMO-Guide.html

Terms and Conditions

Springer Nature journal content, brought to you courtesy of Springer Nature Customer Service Center GmbH (“Springer Nature”).
Springer Nature supports a reasonable amount of sharing of research papers by authors, subscribers and authorised users (“Users”), for small-scale personal, non-commercial use provided that all copyright, trade and service marks and other proprietary notices are maintained. By accessing, sharing, receiving or otherwise using the Springer Nature journal content you agree to these terms of use (“Terms”). For these purposes, Springer Nature considers academic use (by researchers and students) to be non-commercial.
These Terms are supplementary and will apply in addition to any applicable website terms and conditions, a relevant site licence or a personal subscription. These Terms will prevail over any conflict or ambiguity with regards to the relevant terms, a site licence or a personal subscription (to the extent of the conflict or ambiguity only). For Creative Commons-licensed articles, the terms of the Creative Commons license used will apply.
We collect and use personal data to provide access to the Springer Nature journal content. We may also use these personal data internally within ResearchGate and Springer Nature and as agreed share it, in an anonymised way, for purposes of tracking, analysis and reporting. We will not otherwise disclose your personal data outside the ResearchGate or the Springer Nature group of companies unless we have your permission as detailed in the Privacy Policy.
While Users may use the Springer Nature journal content for small scale, personal non-commercial use, it is important to note that Users may not:

1. use such content for the purpose of providing other users with access on a regular or large scale basis or as a means to circumvent access control;
2. use such content where to do so would be considered a criminal or statutory offence in any jurisdiction, or gives rise to civil liability, or is otherwise unlawful;
3. falsely or misleadingly imply or suggest endorsement, approval , sponsorship, or association unless explicitly agreed to by Springer Nature in writing;
4. use bots or other automated methods to access the content or redirect messages
5. override any security feature or exclusionary protocol; or
6. share the content in order to create substitute for Springer Nature products or services or a systematic database of Springer Nature journal content.

In line with the restriction against commercial use, Springer Nature does not permit the creation of a product or service that creates revenue, royalties, rent or income from our content or its inclusion as part of a paid for service or for other commercial gain. Springer Nature journal content cannot be used for inter-library loans and librarians may not upload Springer Nature journal content on a large scale into their, or any other, institutional repository.
These terms of use are reviewed regularly and may be amended at any time. Springer Nature is not obligated to publish any information or content on this website and may remove it or features or functionality at our sole discretion, at any time with or without notice. Springer Nature may revoke this licence to you at any time and remove access to any copies of the Springer Nature journal content which have been saved.
To the fullest extent permitted by law, Springer Nature makes no warranties, representations or guarantees to Users, either express or implied with respect to the Springer nature journal content and all parties disclaim and waive any implied warranties or warranties imposed by law, including merchantability or fitness for any particular purpose.
Please note that these rights do not automatically extend to content, data or other material published by Springer Nature that may be licensed from third parties.
If you would like to use or distribute our Springer Nature journal content to a wider audience or on a regular basis or in any other manner not expressly permitted by these Terms, please contact Springer Nature at

onlineservice@springernature.com